

# Chain-length-dependent correlated molecular motion in polymers

Matthew Reynolds<sup>1</sup>, Daniel L. Baker<sup>1</sup>, Peter D. Olmsted<sup>2</sup>, and Johan Mattsson<sup>1\*</sup>

<sup>1</sup>*School of Physics and Astronomy, University of Leeds, Leeds LS2 9JT, United Kingdom and*

<sup>2</sup>*Department of Physics and Institute for Soft Matter Synthesis and Metrology, Georgetown University, Washington DC, 20057*

(Dated: May 7, 2024)

We show how dynamic heterogeneities (DH), a hallmark of glass-forming materials, depend on chain flexibility and chain length in polymers. For highly flexible polymers, a relatively large number of monomers ( $N_c \sim 500$ ) undergo correlated motion at the glass transition temperature  $T_g$ , independent of molecular weight ( $M$ ). In contrast, less flexible polymers show a complex  $N_c(M)$  behaviour divided into three regimes, consistent with observation in both  $T_g(M)$  and chain conformational structure. For short oligomers ( $\lesssim 2$  Kuhn steps), a transition from mainly *intermolecular* correlations and  $N_c \sim 200$ , to strongly *intramolecular* correlations and  $N_c < 50$  (roughly the molecular size) is observed; for longer chains,  $N_c$  increases weakly, before saturating. For poly(methyl methacrylate), a remarkable similarity is found between  $N_c(M)$  and the  $M$ -dependent ratio of the activation barriers of the structural ( $\alpha$ ) and secondary ( $\beta$ ) relaxations. Our results suggest a link between the DH length-scale and the number of  $\beta$  relaxation events jointly-activated to facilitate the  $\alpha$  relaxation.

Molecular motions in polymer melts slow down during cooling, eventually resulting in the formation of a disordered solid – a glass. The glass transition temperature  $T_g$  is defined as  $\tau_\alpha(T_g) \equiv 100s$  [1], where  $\tau_\alpha(T)$  is the temperature ( $T$ ) dependent structural ( $\alpha$ ) relaxation time [2]. Near  $T_g$ , so called dynamic heterogeneities (DH), in which the local dynamics varies from place to place, become more prominent [3, 4]. Their characteristic length-scale  $\xi_{DH}$  has been determined for both polymeric and non-polymeric liquids [5–9], using nuclear magnetic resonance [10], temperature-modulated differential scanning calorimetry (TMDSC) [11], broadband dielectric spectroscopy (BDS) [9, 12], solvation dynamics [13], single-molecule spectroscopy [14], light scattering [15, 16], or computer simulations [17–23]. The resulting length-scale  $\xi_{DH}(T_g) \sim 1\text{-}5$  nm, which for polymers correspond to 50-500 monomers [7, 9, 24]. Moreover,  $\xi_{DH}$  has been shown to correlate with the activation volume for structural relaxation [15, 24], the volumetric contribution to dynamic fragility (the sensitivity of  $\tau_\alpha(T)$  to a  $T$ -variation near  $T_g$ ), and the properties of the excess in the vibrational density of states compared with the Debye prediction (*i.e.* the Boson peak) [15]. The very few studies that have investigated how polymer chain-length affects DH [9, 25, 26] have not explored the entire range from short oligomers to long-chain polymers.

To address this, we focus here on the effects of chain-length (or molecular weight  $M$ ) on DH. We study four different polymer chemistries: poly(methyl methacrylate) (PMMA); polystyrene (PS); poly(propylene glycol dimethyl ether) (PPG-DME), and poly(dimethyl siloxane) (PDMS). PMMA and PS show relatively high  $T_g$ , dynamic fragility  $m$ , and chain stiffness [27], whereas PPG-DME and PDMS are significantly more flexible polymers characterised by lower  $T_g$  and  $m$ .

DH can be characterised by a “four-point” correlation function  $G_4(\mathbf{r}, t)$  that correlates the relaxation dynamics (probed by two-point correlators) in space and time.

A space-integration of  $G_4(\mathbf{r}, t)$  yields a dynamic susceptibility  $\chi_4(t)$ , which quantifies the fluctuations around the average dynamics [4, 19, 22, 28, 29].  $\chi_4(t)$  is typically a non-monotonic function with a peak  $\chi_4^{\max}$  near  $t_{\max} \simeq \tau_\alpha(T)$ , where  $\chi_4^{\max}$  is proportional to the volume of correlated motions, or correspondingly the number of monomer units  $N_c^{(4)}$  that undergo correlated motions. Direct determination of  $\chi_4(t)$  is difficult and has mainly been achieved in simulations [4, 19, 22] and for colloidal systems [30, 31], and recently for a metallic glass-former [32]. However, it has been demonstrated that  $\chi_4(t)$  can be estimated from the temperature dependence of a dynamic susceptibility [28, 29], obtained from broadband dielectric spectroscopy (BDS), rheology, or scattering [28, 29].

The glass transition related dynamics of polymers can typically be divided into three distinct regimes [33, 34], corresponding to (I) short oligomers ( $\lesssim 2$  Kuhn steps), (II) chains with  $\sim 2\text{-}20$  Kuhn steps, and (III) long chains. These regimes are captured in the  $T_g(M)$  behaviour (segmental dynamics) and in the chain structure [34]. The inset to Fig. 2 shows an example for PMMA, illustrating  $T_g(M)$  (open black symbols) and the  $M$ -dependent single-molecule aspect ratio  $\Lambda^2(M) = \lambda_3(M)^2/\lambda_1(M)^2$  (solid green symbols), where  $\lambda_3^2$  and  $\lambda_1^2$  are the largest and smallest eigenvalues, respectively, of the average conformational tensor [34]. The regime I-II boundary at  $M^*$  is clearly manifested as both a kink in  $T_g(M)$  and a peak in  $\Lambda^2$ , where the latter is due to chain folding occurring for  $M \gtrsim M^*$  [34]. For long chains in regime III ( $> M^{**}$ ),  $\Lambda^2$  approaches the Gaussian chain value of  $\approx 12$ .

We employ two approaches to determine the number of dynamically correlated units involved in the  $\alpha$  relaxation. The first approach, proposed by Donth [11, 35], yields the number of correlated units  $N_c(T \sim T_g)$  from the thermal fluctuations measured near  $T_g$  using TMDSC. The second approach, proposed by Berthier *et al.* [28], estimates

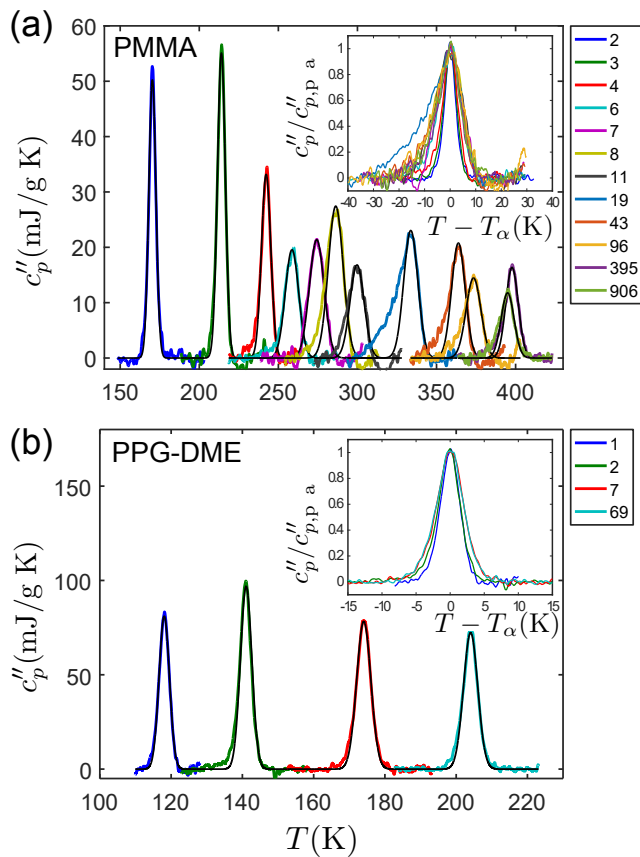


FIG. 1. The imaginary part of the  $T$ -dependent specific heat  $c_p''(T)$  for (a) PMMA and (b) PPG-DME. The legends show the degree of polymerisation  $n$ . The peak in  $c_p''(T)$  corresponds to the response due to the structural  $\alpha$  relaxation, with Gaussian fits (black lines). The insets show all  $c_p''(T)$  data normalized and centered on the peak temperature  $T_\alpha$ .

$\chi_4$  from the temperature-dependence of the complex permittivity measured using BDS, which then yields  $N_c(T)$ .

Using the first approach [11], the mean square temperature fluctuations  $\delta T^2$  within a rearranging region are related to the breadth  $\delta T$  of the calorimetric glass transition response in  $c_p''$ , and in turn to the volume  $V_c$  of the correlated regions by  $V_c = k_B T_\alpha^2 \Delta c_V^{-1} / (\rho \delta T^2)$  [3, 11].

The peak in  $c_p''(T)$  occurs at  $T_\alpha$ ,  $\rho$  is the mass density, and  $\Delta c_V^{-1} = c_{V,g}^{-1} - c_{V,l}^{-1}$  is the difference in reciprocal isochoric specific heat of the glassy and liquid states at  $T_\alpha$ . Hence, the number of monomers  $N_c = \rho V_c N_A / M_0$  taking part in correlated motion can be estimated as

$$N_c(M, P) = \frac{k_B N_A T_\alpha^2 \Delta c_V^{-1}}{M_0 \delta T^2}, \quad (1)$$

where  $N_A$  is Avogadro's number,  $M_0$  is the monomer molar mass, and  $P$  is the period of the TMDSC oscillation.

TMDSC measurements were performed on PMMA, PS, PPG-DME, and PDMS, as described in the Supplementary Material [36], yielding the complex specific heat capacity  $c_p^*(T) = c_p'(T) - i c_p''(T)$ . The real component

$c_p'(T)$  shows the step observed across the glass transition (see Fig. S1 of [36]), which yields  $\Delta c_p^{-1}$ . The imaginary component  $c_p''(T)$  shows a peak at the transition temperature  $T_\alpha$ ;  $T_\alpha$  and  $\delta T$  were calculated based on a Gaussian fit to  $c_p''(T)$  as in [37]. We follow the literature [7, 9, 38] and approximate  $c_V \approx c_p$ , which slightly overestimates  $N_c$  but does not affect our conclusions [39]

$c_p''(T; M)$  are shown for PMMA and PPG-DME in Figure 1, measured using a modulation period  $P = 60$ s, corresponding to  $\tau_\alpha \approx 10$ s. For both polymers, a clear increase in the peak temperatures  $T_\alpha$  is observed with increasing  $M$ . The variation with molecular weight is smaller for PPG-DME than for PMMA, which is expected due to the higher chain flexibility of PPG-DME [34] that leads to a smaller variation in  $T_g$ .

The amplitude-renormalized  $c_p''(T)$  peaks (insets to Fig. 1) show a broadening  $\delta T$  with increasing  $M$ . The asymmetry for longer PMMA chains is due to vitrification effects below  $T_g$  [37], so the temperature range of the Gaussian fit was limited to  $T \gtrsim T_g$ . Qualitatively similar trends ( $T_\alpha$  and  $\delta T$  increasing with  $M$ ) are observed for PS and PDMS (see Fig. S3 in [36]). The increase in  $\delta T$  is more prominent in PMMA and PS than in the more flexible PPG-DME and PDMS, which we discuss below.

The results for  $N_c(M)$  are shown for PMMA in Figure 2(a). We find that  $N_c(M)$  falls dramatically in regime I from  $N_c \sim 220$  for the dimer to  $N_c < 50$  as the regime II boundary at  $M^*$  is approached. This demonstrates that near  $T_g$  the  $\alpha$  relaxation dynamics for short oligomers (within regime I) are highly correlated, and since these molecules are very short, the dynamics are strongly intermolecular. This is illustrated in Fig. 2(b), which shows  $N_p(M) = N_c(M)/n(M)$ , where  $n$  is the degree of polymerisation. For short chains  $N_p(M)$  is roughly the  $M$ -dependent number of correlated molecules. We observe that  $N_p$  drops from  $N_p \sim 110$  for the dimer to  $N_p \sim \mathcal{O}(1)$  near  $M^*$ , reflecting strongly intramolecular behaviour for  $M \gtrsim M^*$ . Figure 2(a) shows that  $N_c$  increases slightly with  $M$  in regime II to reach  $N_c \sim 60$  in regime III. Thus, the number of correlated monomers  $N_c(M)$ , as well as  $T_g(M)$  and the chain structure  $\Lambda^2(M)$  (inset of Fig. 2(b)) all show distinct changes in behaviour for similar characteristic molecular weights.

We compare  $N_c(M)$  for all four polymers in Fig. 3. The stiffer polymers (PMMA and PS) show a sharp decrease of  $N_c(M)$  in regime I, followed by a weak increase in regime II. However, the more flexible polymers (PPG-DME and PDMS) show a roughly constant  $N_c(M)$ , which exceeds that of the shortest PMMA and PS oligomers. For PPG-DME and PDMS,  $N_c$  is larger than the degree of polymerisation  $n$ , *i.e.*  $N_p > 1$ , until regime III is reached.

The rotational dihedral barriers of PPG-DME and PDMS (respectively  $\lesssim 1.0$  [40] and  $0.6$  kcal/mole [41]) are significantly smaller than those of PMMA and PS (respectively  $2.8$  [42] and  $3$  kcal/mole [41]), and the O-

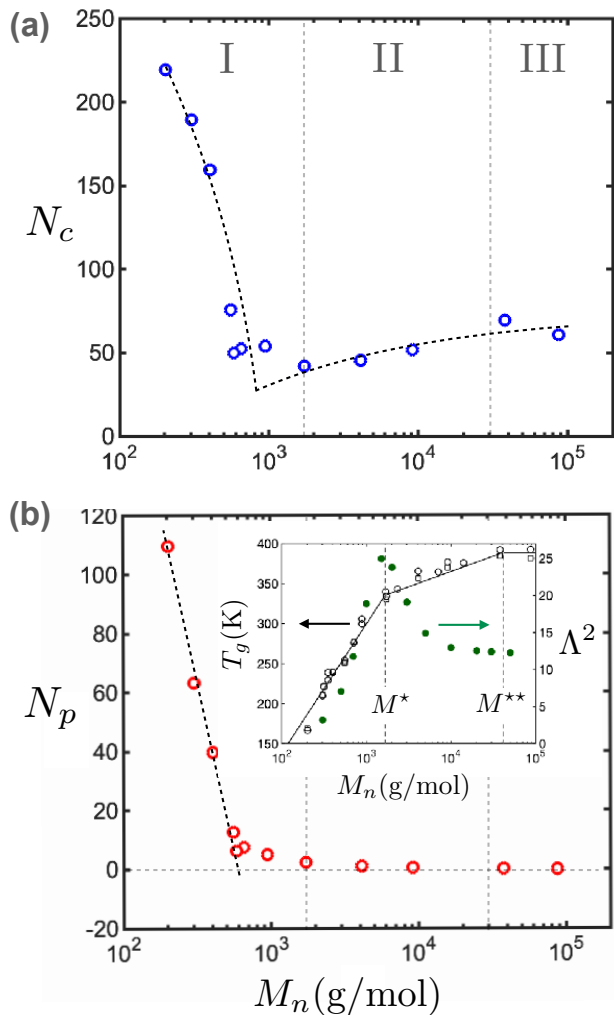


FIG. 2. (a) The number of monomers  $N_c$  involved in the  $\alpha$  relaxation at  $T_\alpha \simeq T_g$  for PMMA, determined using TMDSC. (b)  $N_p \equiv N_c/n$ , where  $n$  is the degree of polymerisation. For short chains, where the behaviour is intermolecular,  $N_p$  is roughly the number of molecules involved in the  $\alpha$  relaxation. In contrast,  $N_p \sim 1$  for  $M \sim M^*$ , which demonstrates the importance of intramolecular dynamics for  $M \geq M^*$ . The dashed lines are guides to the eye. The inset of (b) shows the  $M$ -dependence of  $T_g$  (left) and the average polymer aspect ratio  $\Lambda^2$  (right).

Si-O bending energy for PDMS is notoriously weak [43]. This suggests that intramolecular constraints are much weaker for PDMS and PPG-DME, which explains why chain connectivity, and thus chain-length, do not significantly influence their  $\alpha$  relaxation behaviour, as demonstrated by the nearly  $M$ -independent  $N_c \sim 300-700 \gg n$ .

For non-polymeric glass-formers and for short oligomers (in regime I), the molecular motions linked to the structural  $\alpha$  relaxation are dominated by translational degrees of freedom (DOF). As chains with relatively high dihedral barriers (such as PMMA or PS) grow, the number of DOF available for molecular motions

is reduced, by exchanging three intermolecular translational DOF for one dihedral intramolecular DOF (per additional degree of polymerization) [44]. This is accompanied by a change of the  $\alpha$  relaxation character from mainly intermolecular to highly intramolecular. This is directly illustrated near the regime I-II crossover ( $M \sim M^*$ ), where chain folding takes place [34] and  $N_c \sim n$ . Correspondingly, as chains grow within regime I, less cooling is required for dynamic arrest to occur, meaning that fewer monomers are involved in correlated motions at  $T_g$ , as shown in Fig 3.

We next use BDS to estimate the number of monomers within a dynamic correlation volume, using the fluctuation-dissipation-based approach of Berthier *et al.* [28, 29]. They showed that a “three-point” dynamic susceptibility is a lower bound to  $\chi_4$ , so that the number of dynamically correlated monomers  $N_c^{(4)}(T)$  are

$$N_c^{(4)}(T) \approx \frac{k_B N_A}{m_0 \Delta c_p} T^2 \max_{\omega} \left\{ \left| \frac{d\chi(\omega, T)}{dT} \right| \right\}^2, \quad (2)$$

where  $m_0 \Delta c_p$  is the difference in isobaric monomer molar heat capacity between the liquid and glass, and  $\chi(\omega, T) = [\varepsilon'(\omega, T) - \varepsilon_\infty(T)] / [\varepsilon'(0, T) - \varepsilon_\infty(T)]$  is the normalized dynamic susceptibility [29].

Here,  $\varepsilon'(\omega, T)$  is the real component of the complex permittivity and  $\varepsilon_\infty(T)$  is its high-frequency limit. The structural relaxation times  $\tau_\alpha(T)$  associated with the response  $\chi(\omega, T)$  were determined using the fitting approach described in [36], which allowed conversion from  $N_c^{(4)}(T)$  to  $N_c^{(4)}(\tau_\alpha)$ .

Fig. 4 shows  $N_c^{(4)}(\tau_\alpha)$  for PMMA and PPG-DME from

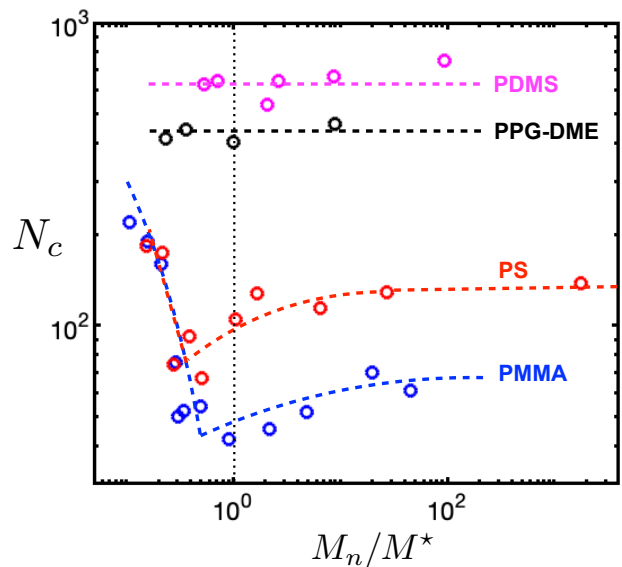


FIG. 3. Comparison of the number of correlated monomers  $N_c$  involved in the  $\alpha$  relaxation for four different polymers as a function of molecular weight  $M_n$ , scaled by the molecular weight  $M^*$  separating regimes I and II.

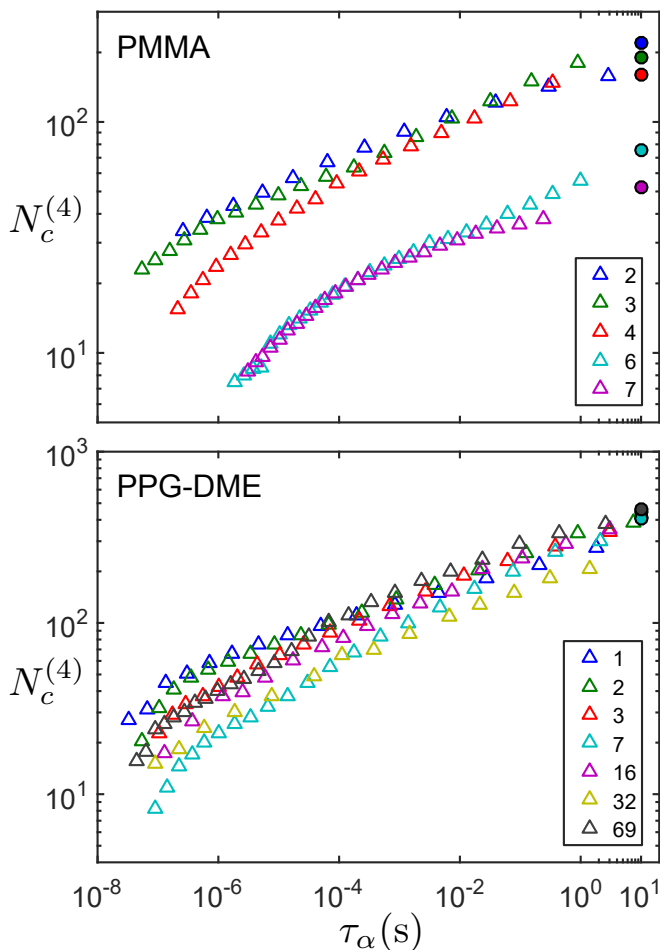


FIG. 4. The number of monomers  $N_c^{(4)}$  ( $\Delta$ ) undergoing correlated motion during the structural  $\alpha$  relaxation for (a) PMMA and (b) PPG-DME, determined using BDS, as a function of the  $\alpha$  relaxation time  $\tau_\alpha$ , for  $n$  noted in the legends. The extrapolation of  $N_c^{(4)}$  to  $\tau_\alpha = 10$  s agrees with the corresponding value  $N_c(\tau_\alpha = 10$  s) from TMDSC ( $\bullet$ ).

BDS data (open symbols), compared with  $N_c$  calculated for  $\tau_\alpha \approx 10$  s from TMDSC data (solid symbols). In both cases, extrapolation of the BDS data shows that  $N_c^{(4)}(10\text{s}) \simeq N_c$ . For PMMA,  $N_c^{(4)}(\tau_\alpha)$  was only calculated for oligomers ( $n = 2-7$ ), since for longer chains the  $\alpha$  relaxation response is increasingly obscured by a strong secondary  $\beta$  relaxation [34], hindering an accurate determination of  $\chi(\omega, T)$ . The corresponding plots for PS and PDMS are shown in Fig. S7 of [36]. For PDMS we generally find good correspondence between  $N_c^{(4)}(10\text{s})$  and  $N_c$ . For PS, a so-called “excess wing” [45, 46] on the high-frequency flank of the  $\alpha$  relaxation obscures the  $\alpha$  response [47], which increases the uncertainty in the absolute values of  $N_c^{(4)}(\tau_\alpha)$ . However,  $N_c^{(4)}$  increases monotonically with  $\tau_\alpha$ , and both  $N_c^{(4)}$  and  $N_c$  show a similar variation with chain-length for  $\tau_\alpha \sim 10$  s.

To further investigate the  $M$ -dependence of  $N_c$  ob-

served for PMMA and PS (Fig. 3), we first note that in addition to the structural  $\alpha$  relaxation, glass-formers generally also show a faster  $\beta$  relaxation corresponding to more ‘local’ cooperative motions [34]; there is significant evidence that the two relaxations are intrinsically linked [34, 48].

Molecular relaxations in the glassy state typically follow the Arrhenius law,  $\tau_i = \tau_{0i} \exp[\Delta H_i/RT]$  ( $i = \alpha, \beta$ ), where  $\tau_{0i} \sim 0.1$  ps is a microscopic relaxation time and  $R$  is the gas constant. Since  $\tau_\alpha(T_g) \equiv 100$  s,  $\Delta H_\alpha(M)|_{T=T_g} = RT_g \ln(100\text{s}/\tau_0)$ ; while  $\Delta H_\beta$  is  $T$ -independent. Thus,  $\Delta H_\alpha(M)|_{T=T_g}$  is proportional to  $T_g(M)$ , and both show three regimes in  $M$  [34] (inset to Fig. 2). While  $\Delta H_\alpha(M)$  follows the  $M$ -dependence of  $T_g(M)$ ,  $\Delta H_\beta(M)$  increases with  $M$  in regime I and is nearly  $M$ -independent in regimes II and III [34]. Hence, the ratio  $\mathcal{R}(M)$  obeys the  $M$ -dependencies of both barriers in regime I, but mainly that of the  $\alpha$  barrier in regimes II and III. Remarkably, as shown in Fig. 5, the ratio  $\mathcal{R}(M) \equiv \Delta H_\alpha(M)/\Delta H_\beta(M)$  between the two activation barriers has an  $M$ -dependence very similar to that of  $N_c(M)$ . Notably,  $\mathcal{R}(M) \approx 1$  for  $M \sim M^*$ , which corresponds to the onset of strongly intramolecular behaviour in  $N_c$  (Fig. 2(b)), and suggests a close correspondence between the properties of the  $\alpha$  and the more ‘local’  $\beta$  relaxation (see a detailed discussion in [34]).

Both non-polymeric and long-chain (regime III) polymeric glass-formers often satisfy  $\Delta H_\beta \approx 24RT_g$  [34, 48, 49], which suggests a typical value of the ratio,  $\mathcal{R} \simeq \frac{1}{24} \ln(100\text{s}/\tau_0) \approx 1.4$ , and a direct link between the  $\alpha$  and  $\beta$  relaxations. In fact, as long ago as 1940, Kauzmann and Eyring [50] suggested that flow in polymers results from “flow segments” comprising  $\sim 5-10$  bonds. Numerous studies have since tried to link ‘local’ dynamics, typically on the scale of the flow segment, to the structural  $\alpha$  relaxation [51–56]. We recently suggested that the link between the  $\alpha$  and  $\beta$  relaxations could be explained by *dynamic facilitation* (DF) [23, 57, 58], whereby a ‘local’ relaxation facilitates adjacent relaxations [23, 34]. In polymers near  $T_g$ , we can apply DF to two situations: (1) For oligomers of stiffer polymers (such as PMMA or PS) at  $T \sim T_g$ , dense packing and relatively large dihedral barriers restrict ‘local’ intramolecular motion to arise from cooperative motion, involving a few adjacent dihedral angles. These ‘local’ cooperative rearrangements can propagate along the chain (*intramolecular facilitation*) and facilitate the rearrangement of the entire oligomer, resulting in the  $\beta$  relaxation and its associated enthalpy  $\Delta H_\beta(M)$ . (2) This newly-mobile oligomeric chain can facilitate the mobility of other oligomers through *intermolecular facilitation*, to yield the  $\alpha$  relaxation and its associated activation enthalpy  $\Delta H_\alpha(T_g)$ . For longer chains, chain folding divides the chain into  $\beta$  relaxation “beads”, leading to a near constant  $\Delta H_\beta(M^*)$  for  $M \geq M^*$ . Here, the structural  $\alpha$  relaxation (and thus  $T_g$ ) results

from propagation of mobility through either intramolecular (along the chain) or intermolecular facilitation of the  $\beta$  beads; the nature of the facilitated dynamic coupling varies with chain-length, thus separating  $T_g(M)$  into distinct dynamic regimes.

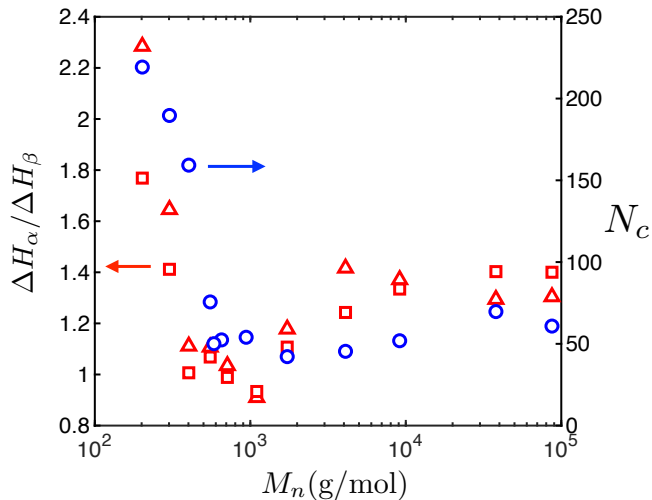


FIG. 5. Comparison between the molecular weight dependent ratio  $\mathcal{R} = \Delta H_\alpha/\Delta H_\beta$  of  $\alpha$  and  $\beta$  activation enthalpies (left axis), and the number of correlated monomers associated with the  $\alpha$  relaxation (right axis) for PMMA.

A hallmark of DF is hierarchical relaxations [57, 58], which lead to a logarithmic relationship between the length-scale  $\ell$  separating fundamental excitations (relaxations) with energy  $\Delta E_\sigma$ , and the activation barrier  $\Delta E = \Delta E_\sigma[1 + \nu \log(\ell/\sigma)]$  of the resulting facilitated relaxation, where  $\nu \sim \mathcal{O}(1)$  is a constant,  $\ell(M)$  is the average length-scale between fundamental relaxations, and  $\sigma(M)$  is their size [23]. By applying this reasoning to  $\Delta H$  data from BDS [34], we recently suggested that the ratio of  $\alpha$  and  $\beta$  barriers at  $T_g$  obeys:

$$\mathcal{R}(M) \equiv \frac{\Delta H_\alpha(M)}{\Delta H_\beta(M)} = \left[ 1 + \nu \log \left( \frac{\ell(M)}{\sigma(M)} \right) \right], \quad (3)$$

which is proportional to the maximum number of  $\beta$  events that act in sync to facilitate the  $\alpha$  relaxation [34, 58]. The simple relation  $\mathcal{R} \simeq \frac{1}{24} \ln(100s/\tau_0)$  breaks down at smaller molecular weights ( $M < M^{**}$ ) in stiff polymers, where intramolecular facilitation plays a role in the structural relaxation.

The remarkable similarity between the  $M$ -dependence of the barrier ratio  $\mathcal{R}(M)$  and  $N_c(M)$  is more difficult to interpret, and even though dynamic facilitation (DF) directly implies dynamic heterogeneities (DH) [23], DH can exist without requiring DF. However, the growing evidence for DF in glass-forming systems [22, 23, 34, 59–62] makes it increasingly important to identify any putative link between DF-properties, such as  $\mathcal{R}(M)$ , and the size of DH, as reflected in  $N_c(M)$  or the corresponding char-

acteristic length-scale  $\xi_{\text{DH}}$  [63]. Recent computer simulations [60, 61] used a swap Monte Carlo technique to access equilibrated temperatures near  $T_g$ , finding that slow regions relax by DF by spreading of mobility from more localised relaxations situated within an ‘excess wing’ on the high-frequency side of the structural  $\alpha$  relaxation response (analogous to our picture of  $\beta$  relaxations facilitating the  $\alpha$  relaxation). Moreover, computer simulations, combined with experiments on a colloidal glass-former [22], found that each ‘particle’ participating in a CRR takes part in many excitations (DF) during the life-time ( $\sim \tau_\alpha$ ) of a CRR, leading the authors to speculate that CRRs form by accumulation of excitations [64]. Also, recent computational studies of a 3D lattice glass model [62] demonstrated that near  $T_g$ , structural relaxation is driven by a small population of mobile particles (characterised by low activation barriers), acting as emerging quasiparticles that drive DH.

Finally, computer simulations and experiments [22, 65–67] have investigated the  $T$ -dependent geometry of DH, with several studies finding that dynamic clusters (CRRs) become increasingly compact near  $T_g$ , so that the characteristic length-scale  $\xi_{\text{DH}} \propto N_c^\gamma$  with  $\gamma \approx 1/3$ . As shown in Fig. S8 of [36], the length-scale  $\xi_{\text{DH}}(M)$ , estimated using the simple approximation of compact CRRs, roughly scales with  $\mathcal{R}(M)$ ; *i.e.* the maximum number of  $\beta$  relaxation ‘beads’ that need to be jointly activated to facilitate the structural  $\alpha$  relaxation (in the DF interpretation [34, 58]). Further work should focus on determining the detailed relationship between dynamic heterogeneities and key molecular elements of dynamic facilitation.

In conclusion, we demonstrate that flexible polymers show a relatively large and  $M$ -independent number of dynamically correlated monomers  $N_c$ , while stiffer polymers show more complex behaviour consistent with the regimes observed in both  $T_g$ , activation enthalpies for chain dynamics, and chain conformational structure; this more complex dynamics results from intramolecular cooperativity necessitated by high dihedral barriers. As short oligomers grow, the dynamics evolve from mainly intermolecular with  $N_c \sim 200$ , to strongly intramolecular with  $N_c < 50$  (similar to the degree of polymerisation), and further increase of  $M$  leads to a weak increase towards an  $M$ -independent limit  $N_c(M \rightarrow \infty)$ . Moreover, we identify a striking similarity between the  $M$ -dependencies of  $N_c$  and the ratio between the structural  $\alpha$  and secondary  $\beta$  relaxation activation barriers, and propose that our results suggest a direct link between the length-scale of dynamic heterogeneities and the relaxation mechanism of dynamic facilitation in polymers.

Our results provide a benchmark for the developments of new theories and models of glass-formation in polymers, and the complexity introduced by chain connectivity could provide an important route to elucidating the mechanisms behind vitrification for glass-formers in

general.

We acknowledge the Engineering and Physical Sciences Research Council (EPSRC) for financial support (EP/M009521/1, EP/P505593/1, and EP/M506552/1). PDO thanks Georgetown University and the Ives Foundation for support. We thank Caroline Crauste for helpful discussions.

---

\* k.j.l.mattsson@leeds.ac.uk

- [1] J. C. Dyre, Colloquium: The glass transition and elastic models of glass-forming liquids, *Reviews of modern physics* **78**, 953 (2006).
- [2] Dynamical arrest into a frozen glassy state occurs at a temperature  $T_{\text{dyn}}$  near  $T_g$ , with a lower  $T_{\text{dyn}}$  for a slower cooling rate.
- [3] H. Sillescu, Heterogeneity at the glass transition: a review, *Journal of Non-Crystalline Solids* **243**, 81 (1999).
- [4] L. Berthier, G. Biroli, J.-P. Bouchaud, L. Cipelletti, and W. van Saarloos, eds., *Dynamical heterogeneities in glasses, colloids, and granular media* (Taylor and Francis, New York, 2011).
- [5] E. Donth, The size of cooperatively rearranging regions in polystyrene and styrene-dimethylsiloxane diblock copolymers at the glass transition temperature, *Acta polymerica* **35**, 120 (1984).
- [6] S. Kahle, J. Korus, E. Hempel, R. Unger, S. Höring, K. Schröter, and E. Donth, Glass-transition cooperativity onset in a series of random copolymers poly (n-butyl methacrylate-stat-styrene), *Macromolecules* **30**, 7214 (1997).
- [7] E. Hempel, G. Hempel, A. Hensel, C. Schick, and E. Donth, Characteristic length of dynamic glass transition near  $T_g$  for a wide assortment of glass-forming substances, *The Journal of Physical Chemistry B* **104**, 2460 (2000).
- [8] S. Cerveny, J. Mattsson, J. Swenson, and R. Bergman, Relaxations of hydrogen-bonded liquids confined in two-dimensional vermiculite clay, *The Journal of Physical Chemistry B* **108**, 11596 (2004).
- [9] B. Rijal, L. Delbreilh, and A. Saiter, Dynamic heterogeneity and cooperative length scale at dynamic glass transition in glass forming liquids, *Macromolecules* **48**, 8219 (2015).
- [10] U. Tracht, M. Wilhelm, A. Heuer, H. Feng, K. Schmidt-Rohr, and H. W. Spiess, Length scale of dynamic heterogeneities at the glass transition determined by multidimensional nuclear magnetic resonance, *Physical Review Letters* **81**, 2727 (1998).
- [11] E. Donth, The size of cooperatively rearranging regions at the glass transition, *Journal of Non-Crystalline Solids* **53**, 325 (1982).
- [12] C. Roland, M. Hensel-Bielowka, M. Paluch, and R. Casalini, Supercooled dynamics of glass-forming liquids and polymers under hydrostatic pressure, *Rep. Prog. Phys.* **687**, 1405 (2005).
- [13] N. Ito, K. Duvvuri, D. V. Matyushov, and R. Richert, Solvent response and dielectric relaxation in supercooled butyronitrile, *J. Chem. Phys.* **125**, 024504 (2006).
- [14] N. L. Mandel, T. Rehman, and L. J. Kaufman, Manifestations of static and dynamic heterogeneity in single molecule translational measurements in glassy systems, *J. Chem. Phys.* **157**, 157 (2022).
- [15] L. Hong, V. Novikov, and A. P. Sokolov, Is there a connection between fragility of glass forming systems and dynamic heterogeneity/cooperativity?, *Journal of Non-Crystalline Solids* **357**, 351 (2011).
- [16] L. Hong, P. Gujrati, V. Novikov, and A. Sokolov, Molecular cooperativity in the dynamics of glass-forming systems: A new insight, *The Journal of chemical physics* **131**, 194511 (2009).
- [17] A. I. Melcuk, R. A. Ramos, H. Gould, W. Klein, and R. D. Mountain, Long-lived structures in fragile glass-forming liquids, *Physical review letters* **75**, 2522 (1995).
- [18] J. Horbach, W. Kob, K. Binder, and C. A. Angell, Finite size effects in simulations of glass dynamics, *Physical Review E* **54**, R5897 (1996).
- [19] L. Berthier and G. Biroli, Theoretical perspective on the glass transition and amorphous materials, *Rev. Mod. Phys.* **83**, 587 (2011).
- [20] G. Jung, G. Biroli, and L. Berthier, Predicting dynamic heterogeneity in glass-forming liquids by physics-informed machine learning, *Phys. Rev. Lett.* **130**, 238202 (2023).
- [21] L. Berthier and D. Reichman, Modern computational studies of the glass transition, *Nat. Rev. Phys.* **5**, 102 (2023).
- [22] L. Ortlieb, T. S. Ingebrigtsen, J. E. Hallett, F. Turci, and C. P. Royall, Probing excitations and cooperatively rearranging regions in deeply supercooled liquids, *Nature Communications* **14**, 2621 (2023).
- [23] A. S. Keys, L. O. Hedges, J. P. Garrahan, S. C. Glotzer, and D. Chandler, Excitations are localized and relaxation is hierarchical in glass-forming liquids, *Physical Review X* **1**, 021013 (2011).
- [24] E. Bouthegourd, A. Esposito, D. Lourdin, A. Saiter, and J. Saiter, Size of the cooperative rearranging regions vs. fragility in complex glassy systems: Influence of the structure and the molecular interactions, *Physica B: Condensed Matter* **425**, 83 (2013).
- [25] C. J. Ellison, M. K. Mundra, and J. M. Torkelson, Impacts of polystyrene molecular weight and modification to the repeat unit structure on the glass transition-nanoconfinement effect and the cooperativity length scale, *Macromolecules* **38**, 1767 (2005).
- [26] K. Schröter, S. Reissig, E. Hempel, and M. Beiner, From small molecules to polymers: relaxation behavior of n-butyl methacrylate based systems, *Journal of Non-Crystalline Solids* **353**, 3976 (2007).
- [27] L. Fetters, D. Lohse, D. Richter, T. Witten, and A. Zirkel, Connection between polymer molecular weight, density, chain dimensions, and melt viscoelastic properties, *Macromolecules* **27**, 4639 (1994).
- [28] L. Berthier, G. Biroli, J.-P. Bouchaud, L. Cipelletti, D. El Masri, D. L'Hôte, F. Ladieu, and M. Pierno, Direct experimental evidence of a growing length scale accompanying the glass transition, *Science* **310**, 1797 (2005).
- [29] C. Dalle-Ferrier, C. Thibierge, C. Alba-Simionesco, L. Berthier, G. Biroli, J.-P. Bouchaud, F. Ladieu, D. L'Hôte, and G. Tarjus, Spatial correlations in the dynamics of glassforming liquids: Experimental determination of their temperature dependence, *Physical Review E* **76**, 041510 (2007).
- [30] Y. Rahmani, K. van der Vaart, B. van Dam, Z. Hu,

- V. Chikkadi, and P. Schall, Dynamic heterogeneity in hard and soft sphere colloidal glasses, *Soft Matter* **8**, 4264 (2012).
- [31] E. Weeks, J. C. Crocker, and D. A. Weitz, Short- and long-range correlated motion observed in colloidal glasses and liquids, *J. Phys.: Condens. Matter* **19**, 205131 (2007).
- [32] P. Zhang, J. J. Maldois, Z. Liu, J. Schroers, and P. M. Voyles, Spatially heterogeneous dynamics in a metallic glass forming liquid imaged by electron correlation microscopy, *Nature Communications* **9**, 1129 (2018).
- [33] J. Cowie, Some general features of  $t_g$ - $m$  relations for oligomers and amorphous polymers, *European Polymer Journal* **11**, 297 (1975).
- [34] D. L. Baker, M. Reynolds, R. Masurel, P. D. Olmsted, and J. Mattsson, Cooperative intramolecular dynamics control the chain-length-dependent glass transition in polymers, *Phys. Rev. X* **12**, 021047 (2022).
- [35] E. Donth, *The glass transition: relaxation dynamics in liquids and disordered materials*, Vol. 48 (Springer Science & Business Media, 2013).
- [36] See Supplemental Material at <http://link.aps.org/supplemental/XXX/XXX> for information about the calorimetry, dielectric spectroscopy, and additional data.
- [37] A. Hensel and C. Schick, Relation between freezing-in due to linear cooling and the dynamic glass transition temperature by temperature-modulated dsc, *Journal of non-crystalline solids* **235**, 510 (1998).
- [38] R. Casalini and C. Roland, Effect of regioisomerism on the local dynamics of polychlorostyrene, *Macromolecules* **47**, 4087 (2014).
- [39] Since  $C_p = C_V + TV\lambda^2/\kappa_T$ , where  $\lambda$  is the thermal expansion coefficient and  $\kappa_T$  is the isothermal bulk modulus, the approximation  $C_V \simeq c_p$  will slightly overestimate the number of the correlated monomers from Eq. 1. Hempel *et al.* [7] calculated a correction factor based on data for both small molecular and polymeric glass formers, which if applied would increase the determined correlation volume values by  $\approx 3\%$ . However, since (i) the correction factor is small, (ii) we do not know how the correction varies for the different chemistries, or  $M$ , investigated here, and (iii) a correction will not affect the conclusions of this work, we follow the approach normally used in literature and approximate  $c_V \approx c_p$ .
- [40] G. D. Smith, O. Borodin, and D. Bedrov, Quantum chemistry based force field for simulations of poly (propylene oxide) and its oligomers, *The Journal of Physical Chemistry A* **102**, 10318 (1998).
- [41] A. Agapov and A. P. Sokolov, Size of the dynamic bead in polymers, *Macromolecules* **43**, 9126 (2010).
- [42] P. Sundararajan and P. Flory, Configurational characteristics of poly (methyl methacrylate), *Journal of the American Chemical Society* **96**, 5025 (1974).
- [43] J. S. Smith, O. Borodin, and G. D. Smith, A quantum chemistry based force field for poly (dimethylsiloxane), *The Journal of Physical Chemistry B* **108**, 20340 (2004).
- [44] Bond stretching and bond bending account for the two DOF ‘lost’ upon polymerization, but these DOF do not participate in molecular motions for polymers with high dihedral barriers and large bending energies.
- [45] P. K. Dixon, L. Wu, S. R. Nagel, B. D. Williams, and J. P. Carini, Scaling in the relaxation of supercooled liquids, *Phys. Rev. Lett.* **65**, 1108 (1990).
- [46] J. Hintermeyer, A. Herrmann, R. Kahlau, C. Goiceanu, and E. Rossler, Molecular weight dependence of glassy dynamics in linear polymers revisited, *Macromolecules* **41**, 9335 (2008).
- [47] The excess wing has commonly been attributed to a ‘hidden’  $\beta$  relaxation [12, 68, 69], or alternatively to an intrinsic feature of the  $\alpha$  relaxation [45].
- [48] A. Kudlik, S. Benkhof, T. Blochowicz, C. Tschirwitz, and E. Rössler, The dielectric response of simple organic glass formers, *Journal of molecular structure* **479**, 201 (1999).
- [49] K. Ngai and S. Capaccioli, Relation between the activation energy of the johari-goldstein  $\beta$  relaxation and  $t_g$  of glass formers, *Physical Review E* **69**, 031501 (2004).
- [50] W. Kauzmann and H. Eyring, The viscous flow of large molecules, *J. Am. Chem. Soc.* **62**, 3113 (1940).
- [51] R. F. Boyer, The relation of transition temperatures to chemical structure in high polymers, *Rubber. Chem. Technol.* **36**, 1303 (1963).
- [52] V. A. Bershtein, E. V. M., A. F. Podolsky, and V. A. Stepanov, Interrelationship and common nature of the  $\beta$  relaxation and the glass transition in polymers, *J. Polym. Sci., Polym. Lett. Ed.* **23**, 371 (1985).
- [53] R. H. Boyd, Relaxation processes in crystalline polymers: molecular interpretation - a review, *Polymer* **26**, 1123 (1985).
- [54] K. Ngai and D. Plazek, Relation of internal rotational isomerism barriers to the flow activation energy of entangled polymer melts in the high-temperature arrhenius region, *J. Polym. Sci. and Polym. Phys. Ed.* **23**, 2159 (1985).
- [55] S. Matsuoka and A. Hale, Cooperative relaxation processes in polymers, *J. Appl. Polym. Sci.* **64**, 77 (1997).
- [56] C. M. Roland, S. Hensel-Bielowka, M. Paluch, and R. Casalini, Supercooled dynamics of glass-forming liquids and polymers under hydrostatic pressure, *Rep. Prog. Phys.* **68**, 1405 (2005).
- [57] P. Sollich and M. R. Evans, Glassy time-scale divergence and anomalous coarsening in a kinetically constrained spin chain, *Phys. Rev. Lett.* **83**, 3238 (1999).
- [58] F. Mauch and J. Jäckle, Recursive dynamics in an asymmetrically constrained kinetic ising chain, *Physica A* **262**, 98 (1999).
- [59] A. S. Keys, J. P. Garrahan, and D. Chandler, Calorimetric glass transition explained by hierarchical dynamic facilitation, *PNAS* **110**, 4482 (2013).
- [60] B. Guiselin, C. Scalliet, , and L. Berthier, Microscopic origin of excess wings in relaxation spectra of supercooled liquids, *Nature Physics* **18**, 468 (2022).
- [61] C. Scalliet, B. Guiselin, and L. Berthier, Thirty milliseconds in the life of a supercooled liquid, *Phys. Rev. X* **12**, 041028 (2022).
- [62] Y. Nishikawa and L. Berthier, Collective relaxation dynamics in a three-dimensional lattice glass model, *Physical Review Letters* **132**, 067101 (2024).
- [63] Note that regions of correlated motion are often referred to in the literature as cooperatively rearranging regions (CRR), even though different definitions are often used [22, 28, 70].
- [64] Ortlieb *et al.* [22] defined excitations following the approach used by Keys *et al.* [23].
- [65] S. Albert, T. Bauer, M. Michl, G. Biroli, J.-P. Bouchaud, A. Loidl, P. Lunkenheimer, R. Tourbot, C. Wiertel-Gasquet, and F. Ladieu, Fifth-order susceptibility unveils growth of thermodynamic amorphous order in glass-formers, *Science* **352**, 1308 (2016).
- [66] E. Flenner, H. Staley, and G. Szamel, Universal features

- of dynamic heterogeneity in supercooled liquids, *Physical Review Letters* **112**, 097801 (2014).
- [67] T. Speck, Modeling non-linear dielectric susceptibilities of supercooled molecular liquids, *Journal of Chemical Physics* **155**, 014506 (2021).
- [68] U. Schneider, R. Brand, P. Lunkenheimer, and A. Loidl, Broadband dielectric spectroscopy on glass-forming propylene carbonate, *Phys. Rev. B* **56**, R5713 (1997).
- [69] J. Mattsson, R. Bergman, P. Jacobsson, and L. Börjesson, Chain-length-dependent relaxation scenarios in an oligomeric glass-forming system: from merged to well-separated  $\alpha$  and  $\beta$  loss peaks, *Phys. Rev. Lett.* **90**, 075702 (2003).
- [70] E. Donth, *Journal of Non-Crystalline Solids* **53**, 325 (1982).

## Supplemental Information for: Chain-length-dependent correlated relaxation motion in polymers

Matthew Reynolds<sup>1</sup>, Daniel L. Baker<sup>1</sup>, Peter D. Olmsted<sup>2</sup>, and Johan Mattsson<sup>1\*</sup>

<sup>1</sup>*School of Physics and Astronomy, University of Leeds, Leeds LS2 9JT, United Kingdom and*

<sup>2</sup>*Department of Physics and Institute for Soft Matter Synthesis and Metrology, Georgetown University, Washington DC, 20057*

(Dated: May 7, 2024)

### A. TEMPERATURE-MODULATED DIFFERENTIAL SCANNING CALORIMETRY (TMDSC)

TMDSC measurements were performed using a TA Q2000 DSC with a liquid nitrogen cooling system. A sinusoidal heating/cooling profile with an amplitude of 1 K and a period of  $P = 60$  s (corresponding to  $\tau_\alpha = 60/2\pi \approx 10$  s) was superimposed onto an underlying cooling rate of 0.25 – 0.5 K/min; an exception was made for PDMS for which the experiments were performed on heating following quenching to avoid sample crystallization. An additional necessary step for correcting the phase angle between heat flow and heating rate was carried out following the procedure outlined in Weyer *et al.* [1]. Using this methodology, the complex specific heat capacity,  $c_p^* = c_p' - ic_p''$ , was determined, where the real component  $c_p'$  shows a step and the imaginary component  $c_p''$  is manifested as a peak, as the structural  $\alpha$  relaxation is probed.

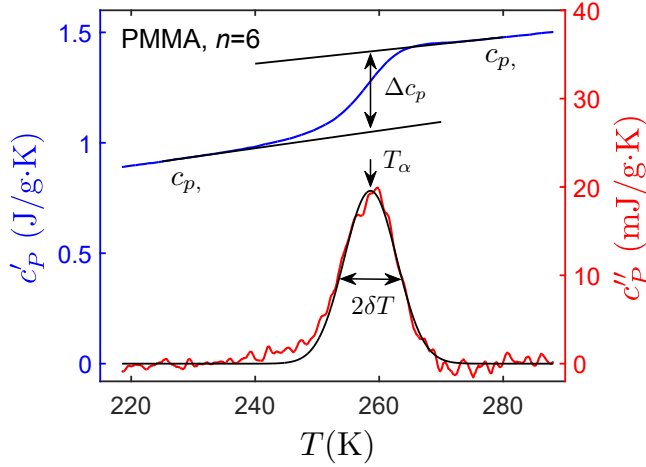


FIG. S1. TMDSC results for PMMA ( $n = 6$ ) across the glass transition, using a modulation period of  $P = 60$  s and an amplitude of  $A = \pm 1$  K.

The results of a typical TMDSC measurement are shown in Fig. S1, where the real and imaginary components of  $c_p^*$  are shown for PMMA with  $n = 6$  ( $M_W = 660$  g/mol).  $c_p'$  shows the typical step observed in a heat

capacity measurement across the glass transition, where  $\Delta c_p^{-1}$  can be determined from the change in the step in  $c_p'(T)$ , as the difference in reciprocal heat capacities of the glass and liquid states at  $T_\alpha$  ( $\Delta c_p^{-1} = c_{p,g}^{-1} - c_{p,l}^{-1}$ ) [2, 3].  $c_p''$  shows a peak, where  $T_\alpha$  and  $\delta T$  can be determined from a fit to a Gaussian function:

$$c_p''(T) = \frac{A}{2\delta T \sqrt{\pi/2}} \exp \left[ -\frac{1}{2} \left( \frac{T - T_\alpha}{\delta T} \right)^2 \right]. \quad (\text{S1})$$

The real component of the complex heat capacity is shown in Fig. S2 for (a) PMMA, (b) PS, (c) PPG-DME, and (d) PDMS, for different degrees of polymerisation,  $n$ . The step in  $c_p'$  at  $T_\alpha$  is akin to that observed in standard DSC, and the trend of increasing  $T_\alpha$ , and thus  $T_g$ , with  $n$  is clearly observed.

The imaginary component of the specific heat  $c_p''$  is shown in Fig. S3 for PMMA, PS, PPG-DME, and PDMS, respectively. The response of the structural ( $\alpha$ ) relaxation manifests as a peak, where  $T_\alpha$  corresponds to the peak temperature. The left-hand figures show the increase in  $T_\alpha$  with increasing  $n$ , with Gaussian (equation S1) fits shown by black lines. The right-hand figure data are amplitude re-normalised and centered on the peak temperature  $T_\alpha$ . An increase in the breadth of the transition ( $\delta T$ ) for increasing  $n$  is observed for all polymers.

Fig. S4 shows the breadth  $\delta T$  (left) and transition step height  $\Delta c_p$  (right) as a function of molecular weight for the four polymer systems.

\* k.j.l.mattsson@leeds.ac.uk

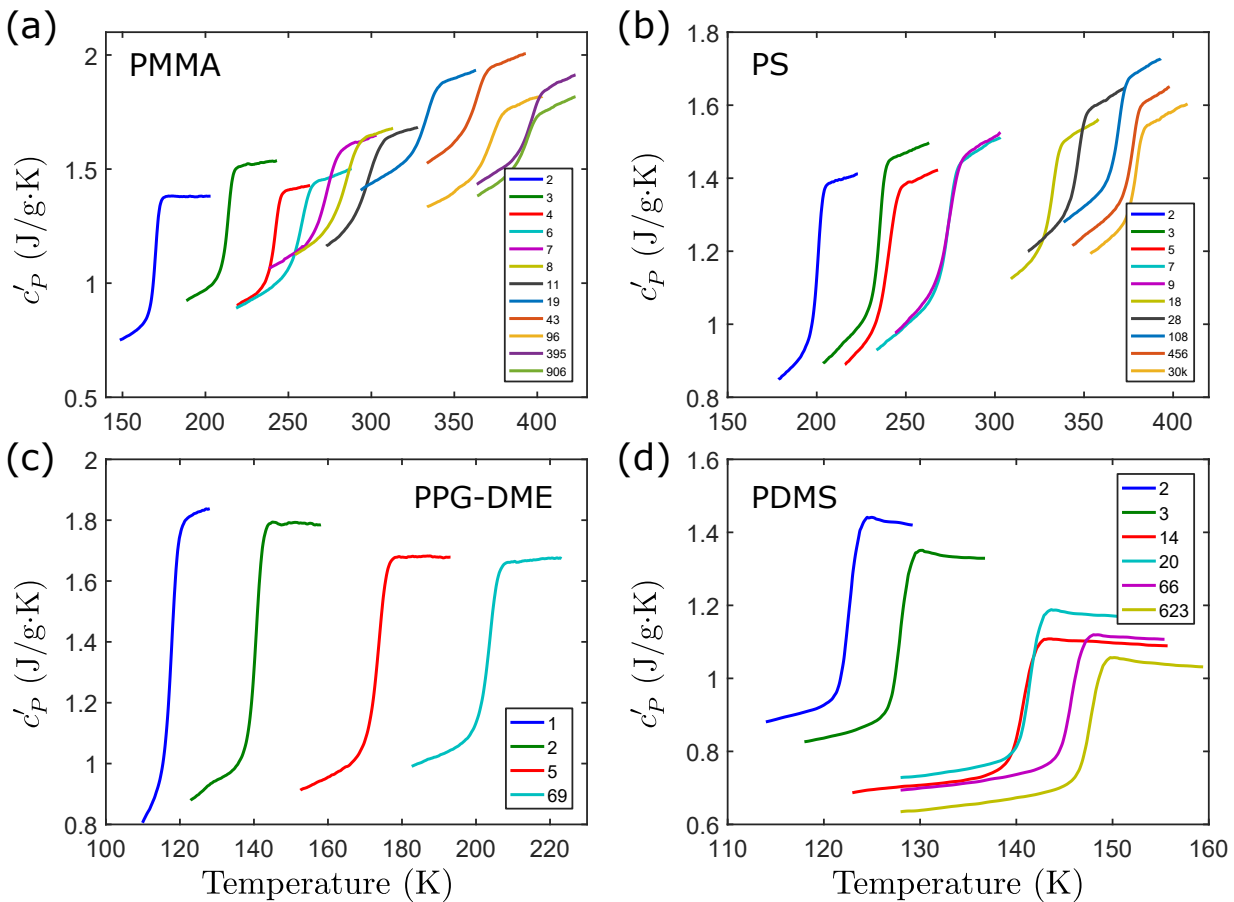


FIG. S2. The real part  $c'_P$  of the specific heat response at  $\omega = 2\pi/60 \text{ s}^{-1}$  for the four polymers. The degrees of polymerization  $n$  are shown in the legends.

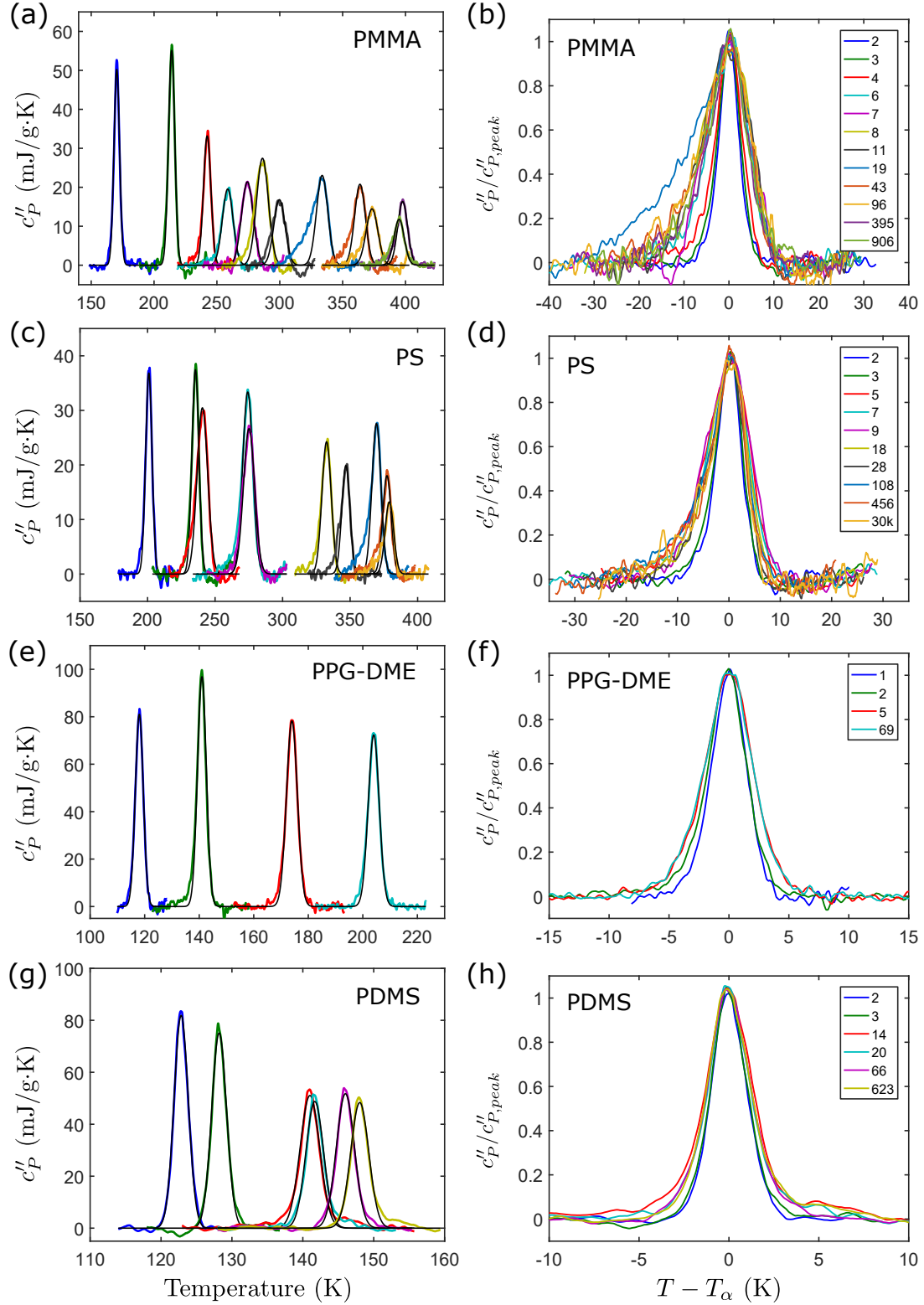


FIG. S3. (Left; **a, c, e, g**)  $c_p''(T)$  ( $P = 60s$ ) with Gaussian fits shown in black; (Right **b, d, f, h**)  $c_p''(T)$  ( $P = 60s$ ) show the data amplitude re-normalised and centered on the peak temperature  $T_\alpha$ , for PMMA, PS, PPG-DME, and PDMS, respectively. The legends show the degree of polymerisation  $n$ .

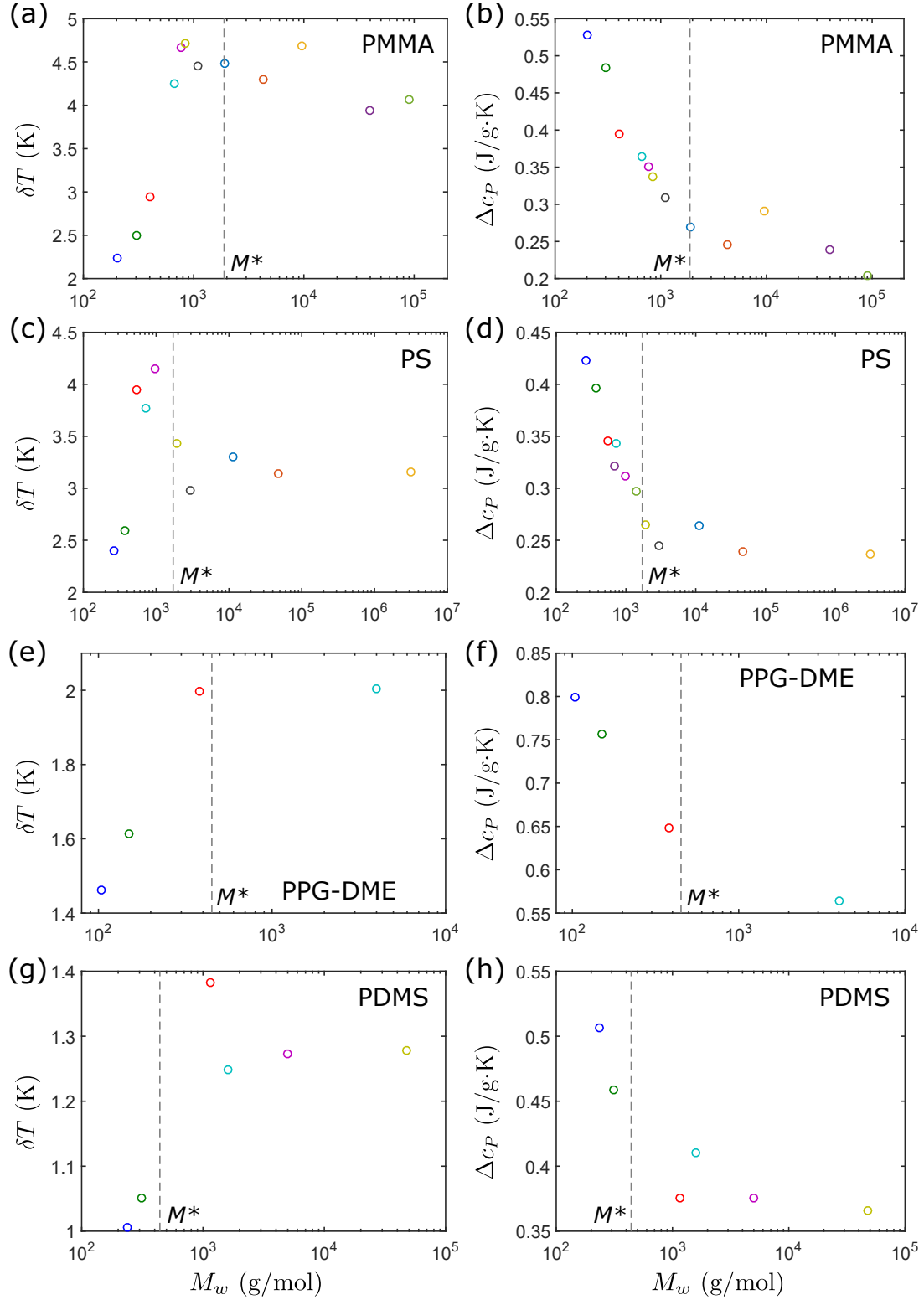


FIG. S4. (Left; a, c, e, g) Breadth of the peak in  $c_p''$  as a function of molecular weight for PMMA, PS, PPG-DME, and PDMS. (Right; b, d, f, h) Step in the real part of the heat capacity  $c_p'$ , as shown in Fig. S1, for PMMA, PS, PPG-DME, and PDMS, as a function of molecular weight.

## B. BROADBAND DIELECTRIC SPECTROSCOPY (BDS)

BDS measurements were performed using a Novocontrol Alpha-A analyser with a Quatro Cryosystem, measuring the complex permittivity  $\varepsilon^*(f)$  for frequencies  $f$  within the range of  $10^{-2} \text{ Hz} \leq \nu \leq 10^6 \text{ Hz}$ , with a temperature accuracy of  $\pm 0.1 \text{ K}$ . To determine  $N_c^{(4)}$  using Eq. 2 of the main paper, the determination of  $T$ -derivatives is required. To ensure that only contributions from the  $\alpha$  relaxation are captured, thus minimising any contributions from additional secondary relaxations, the  $\varepsilon^*(f)$  spectra were fitted by a sum of relaxation contributions:

$$\varepsilon^*(\omega, T) = \frac{-i\sigma(T)}{\omega} + \varepsilon_\infty(T) + \sum_{j=1}^N \frac{\Delta\varepsilon_j(T)}{[1 + (i\omega\tau_j(T))^{m,j}]^{n,j}}, \quad (\text{S2})$$

where  $\omega = 2\pi f$ ,  $\sigma$  is a fitted conductivity, and  $\varepsilon_\infty$  is the high frequency permittivity. The relaxation contributions were described using Havriliak-Negami (HN) functions [4], where  $N = 1, 2$  or  $3$ , depending on how many relaxation modes  $\alpha, \beta, \gamma$  are observed at a given temperature.

The renormalized susceptibility  $\chi(\omega, T)$  is defined from the  $\alpha$  relaxation contribution to  $\varepsilon'(\omega, T)$  S2 by [5]:

$$\chi(\omega, T) = \frac{\varepsilon'(\omega, T) - \varepsilon_\infty(T)}{\varepsilon'(0, T) - \varepsilon_\infty(T)}. \quad (\text{S3})$$

As an example,  $\chi(\omega, T)$  for PDMS with  $n = 2$ , is shown in Fig. S5, where panel (a) shows the values of  $\chi(\omega, T)$  as a function of angular frequency at different temperatures ranging from 121.5 to 128.5 K in steps of 0.5 K. From these data, the calculation of  $T$ -derivatives are necessary to calculate  $N_c^{(4)}$ , where the derivatives were determined using a finite difference approximation. The procedure used to determine  $N_c^{(4)}$  follows that outlined by Dalle-Ferrier *et al.* [5].  $T|d\chi(\omega, T)/dT|$  (*i.e.* the  $T$ -derivative of  $\chi(\omega, T)$  multiplied by  $T$ ), is shown for PDMS ( $n = 2$ ) in Fig. S5(b). An accurate determination of the peak maximum corresponding to each temperature is required to calculate  $N_c^{(4)}(T)$  and Fig. S5(b) illustrates the effect of varying the  $T$ -differences used in the calculation of the corresponding derivatives, where each colour denotes a different  $T$ -step  $\Delta T$  used in the calculation:  $\Delta T = 0.01$  K (black); 1 K (red); 2 K (green); 4 K (blue). Clearly, small  $T$ -steps are required to determine accurate values of the peak maxima.

For our calculations we used  $\Delta T = 0.01 \text{ K}$  ( $T \pm 0.005 \text{ K}$ ), corresponding to the black data in the figure. For each  $T$ ,

we know the  $\alpha$  relaxation HN-parameters, corresponding to  $\chi(\omega, T)$ , from our fitting of the permittivity data. To determine the derivative corresponding to each  $T$ , we assume that the shape of the  $\alpha$  relaxation ( $\chi(\omega, T)$ ) does not change for the very small temperature differences used ( $\Delta T = 0.01 \text{ K}$ ) and the derivative ( $T|d\chi(\omega, T)/dT|$ ) is thus set by the shape and size of the  $\alpha$  relaxation response at each temperature  $T$ , and the difference in  $\alpha$  relaxation time-scale ( $\tau_\alpha(T)$ ) across  $\Delta T$ . For completeness, the  $\alpha$  relaxation time-scale data  $\tau_\alpha(T)$  are shown for all polymers and investigated  $n$  and temperatures in an Arrhenius plot in Fig. S6.

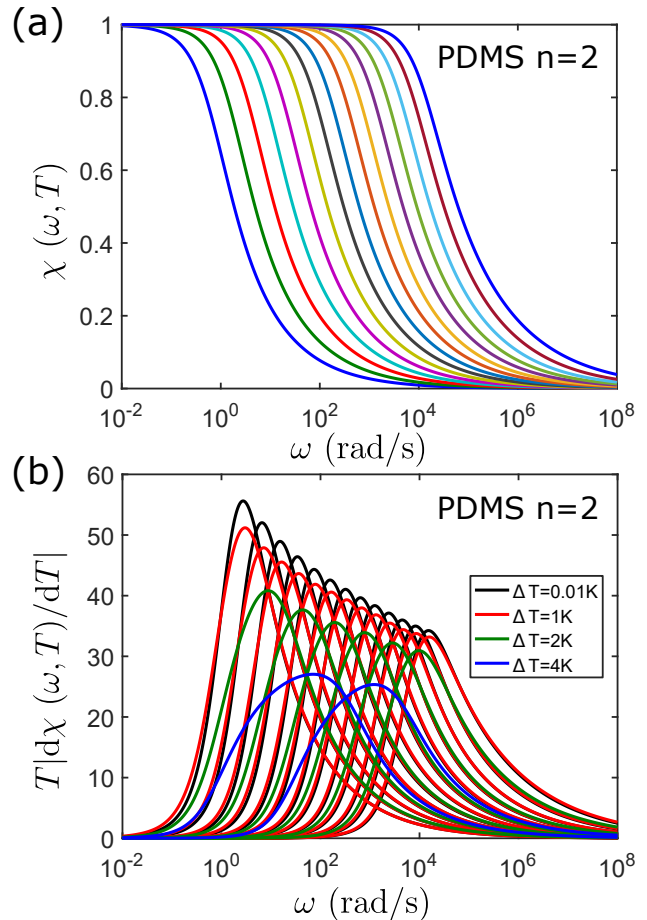


FIG. S5. (a) Normalised susceptibility (calculated using Eq. S2 from Havriliak-Negami  $\alpha$  relaxation parameters) for PDMS (polymerization  $n = 2$ ) as a function of angular frequency  $\omega$ . The different colors correspond to different temperatures, ranging from 121.5 to 128.5 K in steps of 0.5 K. (b)  $T|d\chi(\omega, T)/dT|$  versus  $\omega$  for PDMS ( $n = 2$ ). The different colors represent different temperature differences used to compute the derivatives, as described in detail in the text.

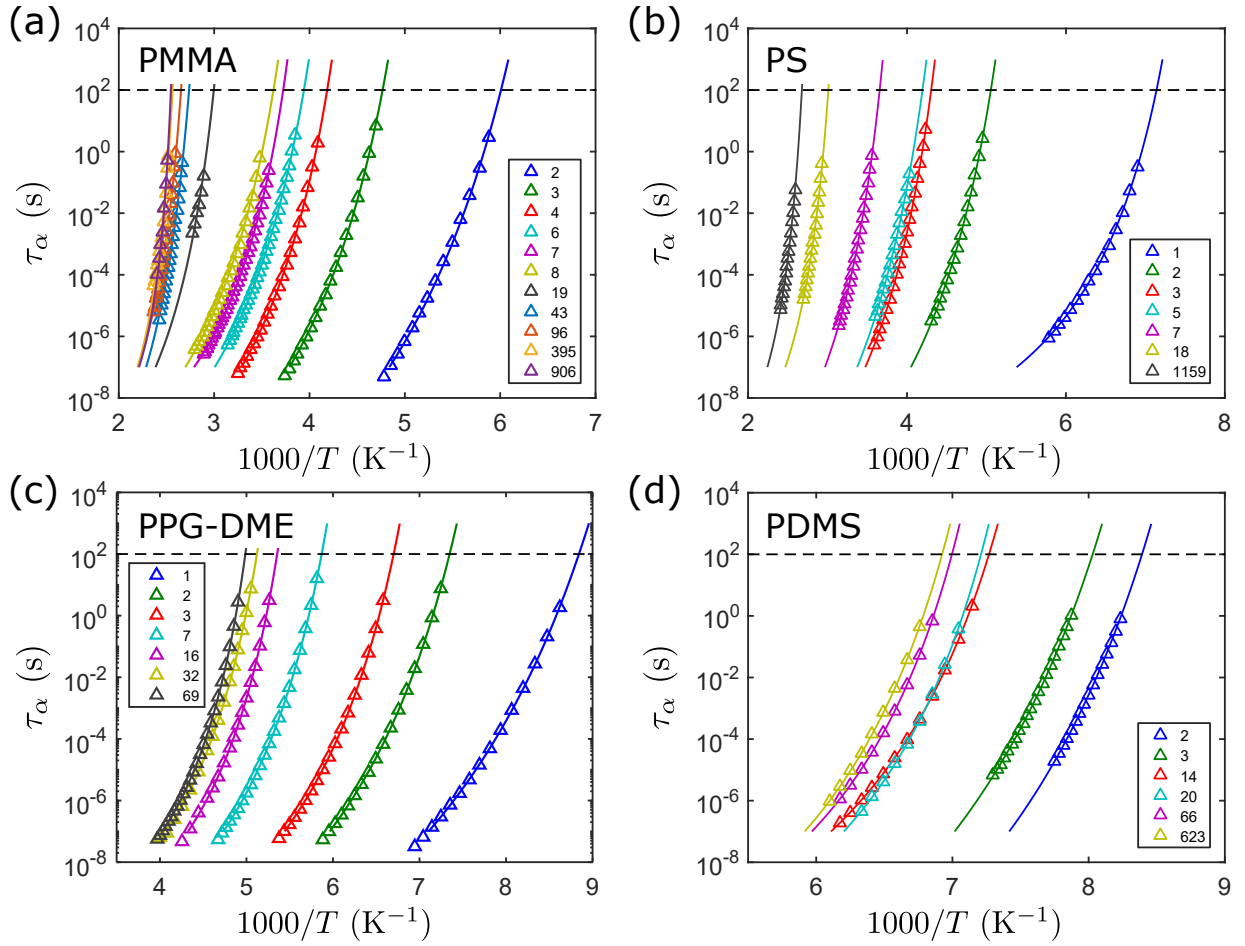


FIG. S6. Arrhenius plots for (a) PMMA, (b) PS, (c) PPG-DME, and (d) PDMS. The solid lines are fits to Vogel Fulcher Tammann (VFT) expressions. The dashed lines mark  $\tau_\alpha=100$  s, since  $T_g \equiv T(\tau_\alpha = 100 \text{ s})$ . The legend shows the degrees of polymerisation  $n$ .

### C. THE NUMBER OF DYNAMICALLY CORRELATED MONOMERS WITHIN THE $\alpha$ RELAXATION

Fig. S7 shows the number of dynamically correlated monomers  $N_c^{(4)}(\tau_\alpha)$  (open symbols) for PMMA, PS, PPG-DME, and PDMS, respectively.  $N_c^{(4)}(\tau_\alpha)$  are calculated from BDS data, as described in the main paper. Also, for each polymer and chain-length, the solid symbol shows the number of dynamically correlated monomers  $N_c$  as determined from TMDSC measurements at a period of 60 s, corresponding to a relaxation time  $\tau_\alpha = 10$  s. The extrapolation of  $N_c^{(4)}(\tau_\alpha)$  to  $\tau_\alpha = 10$  s generally agrees well with  $N_c$ , even though for PS the existence of a so-called “excess wing” [6, 7] on the high-frequency flank of the  $\alpha$  relaxation, measured using BDS, makes the comparisons between the two approaches more difficult. For all four polymer systems,  $N_c^{(4)}$  increases monotonically with  $\tau_\alpha$ , and both  $N_c^{(4)}$  and  $N_c$  show a similar variation with chain-length for  $\tau_\alpha \sim 10$  s.

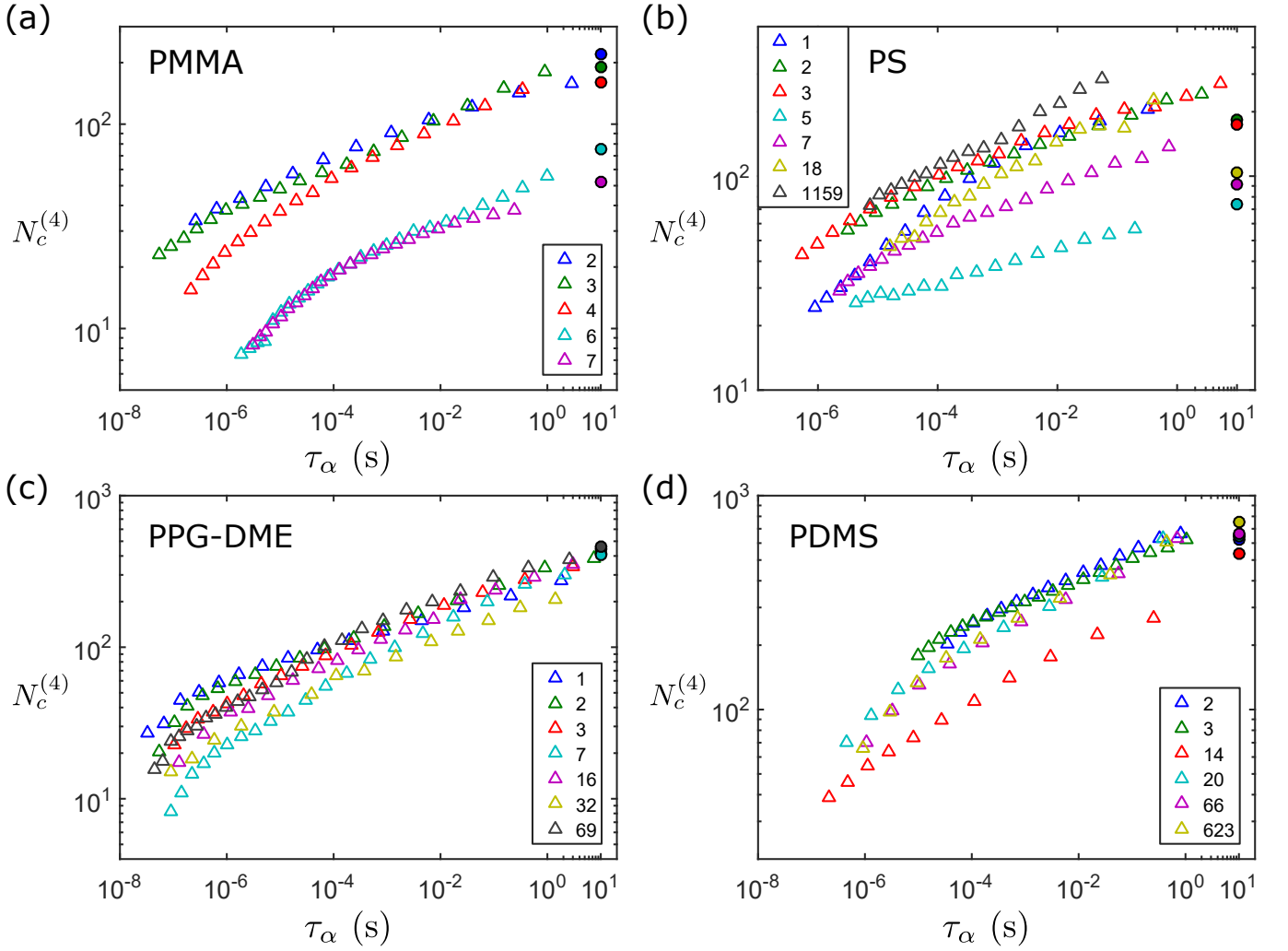


FIG. S7. The number of monomers  $N_c^{(4)}$  ( $\Delta$ ) undergoing correlated motion during the structural  $\alpha$  relaxation for (a) PMMA and (b) PS, (c) PPG-DME, and (d) PDMS, determined using BDS, as a function of the  $\alpha$  relaxation time  $\tau_\alpha$ . The sample degrees of polymerisation  $n$  are listed in the legends. Generally, the extrapolation of  $N_c^{(4)}$  to  $\tau_\alpha = 10$  s agree with the corresponding value  $N_c(\tau_\alpha = 10$  s) from TMDSC ( $\bullet$ ), as described in detail in the text.

#### D. COMPARISON BETWEEN THE ACTIVATION BARRIER RATIO AND THE LENGTH-SCALE OF CORRELATED MOTIONS

If one naively assumes that the  $N_c$  dynamically correlated monomers responsible for the  $\alpha$ -relaxation are distributed homogeneously within a spherical domain of size  $\xi$ , with some volume fraction  $\phi$  (generally  $\phi < 1$ ), then we expect a scaling

$$\xi = \left( \frac{3N_c V_0}{4\pi\phi} \right)^{1/3}, \quad (\text{S4})$$

where  $V_0$  is the monomer volume. This simple argument does not consider a more complex internal structure of the correlation volume, such as a fractal interior. As discussed in the main paper, both computer simulations and experiments [8–11] have studied the  $T$ -dependent geometry of regimes of correlated motions, often observing that dynamic clusters become increasingly compact near  $T_g$  so that the characteristic length-scale  $\xi \propto N_c^\gamma$  with  $\gamma \approx 1/3$ . Thus, in Fig. S8 we compare the length-scale  $\xi = aN_c^{1/3}$  with the enthalpy barrier ratio  $\mathcal{R} = \Delta H_\alpha / \Delta H_\beta$ , and show that these two quantities scale similarly as a function of molecular weight.

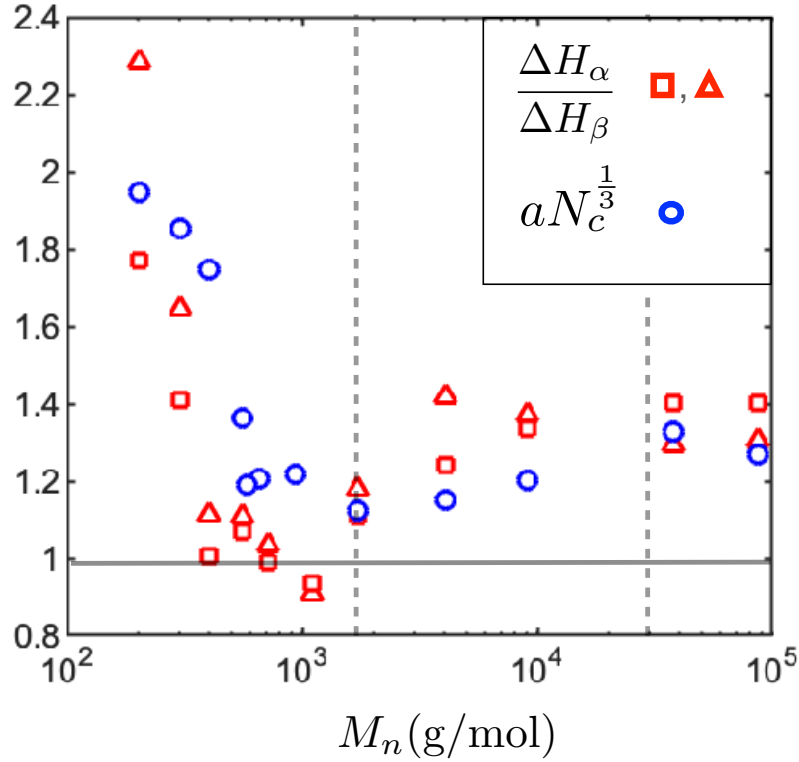


FIG. S8. A demonstration that the ratio of the activation barriers  $\mathcal{R} = \Delta H_\alpha / \Delta H_\beta$  for the  $\alpha$  and  $\beta$  relaxation, respectively, and the lengthscale characterising correlated dynamics  $\xi$  scale similarly with molecular weight, given the assumption  $\xi \sim N_c^{1/3}$ , as discussed in the text.

### E. TABLE OF POLYMER DATA

PMMA					PS					PPG-DME					PDMS				
$n$	$M_w$	PDI	$T_\alpha$	$T_g$	$n$	$M_w$	PDI	$T_\alpha$	$T_g$	$n$	$M_w$	PDI	$T_\alpha$	$T_g$	$n$	$M_w$	PDI	$T_\alpha$	$T_g$
2	202	1.00	170.3	166.4	1	162	1.00	-	140.1	1	104	1.00	118.0	113.1	2	237	1.00	122.8	119.2
3	302	1.00	214.0	209.8	2	266	1.00	201.0	197.8	2	162	1.00	141.0	136.1	3	311	1.00	128.2	124.5
4	402	1.00	242.3	238.9	3	370	1.00	235.4	232.3	3	220	1.00	-	149.2	14	1150	1.27	141.0	137.6
6	660	1.21	258.6	253.7	5	545	1.16	240.6	238.4	7	452	1.02	174.0	170.4	20	1600	1.37	141.7	138.7
7	771	1.18	274.2	268.5	7	725	1.09	274.2	273.5	16	974	-	-	186.8	66	4980	1.29	146.0	142.9
8	840	1.44	286.2	276.1	9	970	1.12	275.2	-	32	1902	-	-	195.3	623	46200	1.12	148.0	144.4
11	1100	1.17	299.7	-	18	1920	1.08	332.6	332.3	69	4048	1.05	204.0	200.5					
19	1900	1.10	333.7	333.7	28	2960	1.04	346.9	-										
43	4300	1.05	363.8	365.3	108	11300	1.02	369.5	-										
96	9590	1.05	373.4	377.0	456	47500	1.03	377.3	-										
395	39500	1.04	397.7	390.1	1159	121k	1.04	-	373.6										
906	90600	1.04	394.9	392.7	30k	3.15M	1.05	379.1	-										

TABLE I. Sample details, including the polydispersity index PDI. Molecular weights  $M_w$  are in g/mol and temperatures  $T_g$  and  $T_\alpha$  are in Kelvin. The temperature  $T_\alpha$  is determined using TMDSC where  $\tau_\alpha = P/2\pi \approx 10$ s ( $P = 60$ s is the modulation period) and  $T_g$  is determined from BDS VFT fits using the criterion  $\tau_\alpha(T_g) = 100$ s.

[1] S. Weyer, A. Hensel, and C. Schick, *Thermochimica acta* **304**, 267 (1997).

[2] A. Hensel and C. Schick, *Journal of non-crystalline solids*

- 235**, 510 (1998).
- [3] E. Hempel, G. Hempel, A. Hensel, C. Schick, and E. Donth, *The Journal of Physical Chemistry B* **104**, 2460 (2000).
- [4] D. L. Baker, M. Reynolds, R. Masurel, P. D. Olmsted, and J. Mattsson, *Phys. Rev. X* **12**, 021047 (2022).
- [5] C. Dalle-Ferrier, C. Thibierge, C. Alba-Simionesco, L. Berthier, G. Biroli, J.-P. Bouchaud, F. Ladieu, D. L'Hôte, and G. Tarjus, *Physical Review E* **76**, 041510 (2007).
- [6] P. K. Dixon, L. Wu, S. R. Nagel, B. D. Williams, and J. P. Carini, *Phys. Rev. Lett.* **65**, 1108 (1990).
- [7] J. Hintermeyer, A. Herrmann, R. Kahlau, C. Goiceanu, and E. Rossler, *Macromolecules* **41**, 9335 (2008).
- [8] L. Ortlieb, T. S. Ingebrigtsen, J. E. Hallett, F. Turci, and C. P. Royall, *Nature Communications* **14**, 2621 (2023).
- [9] S. Albert, T. Bauer, M. Michl, G. Biroli, J.-P. Bouchaud, A. Loidl, P. Lunkenheimer, R. Tourbot, C. Wiertel-Gasquet, and F. Ladieu, *Science* **352**, 1308 (2016).
- [10] E. Flenner, H. Staley, and G. Szamel, *Physical Review Letters* **112**, 097801 (2014).
- [11] T. Speck, *Journal of Chemical Physics* **155**, 014506 (2021).